Proceedings of the 10th International Conference on Fluid Flow, Heat and Mass Transfer (FFHMT'23)
Ottawa, Canada – June 07-09, 2023
Paper No. 171
DOI: 10.11159/ffhmt23.171

Hydrodynamic Profiles of Computed Tomography-Scanned Polydispersed Beds Produced By Sieving

Stylianos Kyrimis[1,2], Robert Raja[2], Lindsay-Marie Armstrong[1]
[1]School of Engineering, University of Southampton, UK, SO17 1BJ
[2]School of Chemistry, University of Southampton, UK, SO17 1 BJ
s.kyrimis@soton.ac.uk, l.armstrong@soton.ac.uk

Abstract **–** Computational Fluid Dynamics (CFD) models are a valuable tool for design, optimization, and scaling-up of fixed bed chemical reactors. However, the realistic representation of the catalytic bed structure and the mesh quality of the 3D geometry is of paramount importance to improve the accuracy of CFD models. For the former, computed tomography (CT) is a non-destructive method to map and generate the internal structure of actual fixed bed reactors, formed by catalytic particles produced by sieving, thus directly coupling experiments with CFD models. Due to the local topological complexity of these beds, however, meshing their entire volume would lead to exhaustive computational demands. To reduce these, a suitable sample section should be selected, which respects the bulk and radial porosity of the full bed as accurately as possible. Three distinct sample sections were quantified here for their accuracy, identifying that, due to the highly heterogeneous nature of the full beds, sample selection is case sensitive. A selected section was then meshed, and its hydrodynamic profile resolved, to evaluate its mesh independency. The results highlight the importance of choosing a suitable bed section and mesh size to reduce the computational demands, minimise the computational errors, and achieve the desired level of solution detail.

Keywords**:** Computational Fluid Dynamics (CFD), polydispersed beds, fixed bed chemical reactors, computed tomography (CT), particle-resolved CFD models (PR-CFD), catalytic particles, SAPO-34

1. Introduction

Optimising fixed bed chemical reactors requires a deep understanding of the interconnected nature of the bed structure with its hydrodynamic profile. For this, Computational Fluid Dynamics (CFD) models play a key role, acting as detailed investigative and optimization tools [1-3], especially when coupled with experimental data to establish their accuracy. This coupling is based on two aspects. The first is experimental data regarding the bed structure characterisation and its hydrodynamic (i.e., velocity profile and pressure drop) profiles. The second is accurately reproducing the packed bed structure as a 3D CFD geometry and mesh. One of the primary methods to achieve the latter is through synthetically generated beds with the Discrete Element Method (DEM), which places particles of arbitrary shapes into a cylindrical container [4, 5].

The interconnection between bed structure and heat and mass transfer characteristics has been studied primarily through DEM-generated monodisperse spherical beds [6-9]. Tobiś investigated both experimentally and computational the turbulent flow of air through packed beds of homogeneous spheres [10, 11], concluding that the local bed structure has a significant influence on the hydrodynamic profile of the flow. Bai *et al.* investigated both experimentally and computationally the pressure drop within packed beds of both spheres and cylinders [12]. Both a laboratory-scale reactor (153 particles) and a plant-scale reactor (up to 1545 particles) were generated by DEM and simulated with CFD [12]. To reduce the computational resources, a small section of the industrial scale reactor was chosen. They identified that for the bed section to be an accurate representation, its porosity should be as close as possible to that of the full bed. Otherwise, even a 10% porosity deviation between the physical and the generated bed could lead to a 30% deviation in the pressure drop predictions [12].

Recent DEM-CFD studies consider more complex particle form aspects, such as shape and orientation, with particles being modelled as cylinders, Raschig rings and trilobes, to name a few [13-16]. Zhang *et al.* investigated polydispersed cylindrical beds, where the particle size within the bed follows a Gaussian distribution [17]. These polydispersed beds were more loosely packed compared to monodispersed beds [17]. Radial porosity profiles near the wall followed similar trends for the mono- and polydispersed beds, however the two profiles deviated near the bed centre. By utilising the polydispersed bed as a CFD geometry, they observed that flow profiles within the interparticle pores are highly heterogeneous [17]. Boccardo *et al.* synthetically generated beds of spheres, cylinders, and trilobes and compared their accuracy, in terms of their

bed structure and flow profiles, with experimental data [18]. Particle size heterogeneity was also introduced. The geometries were utilised for CFD simulations, with the results being compared to theoretical correlations, demonstrating their accuracy [18]. Special focus was put into identifying a suitable section of the full bed to reduce the mesh sizes and the computational demands of the complex bed structures. They identified that a suitable bed section should respect both the bulk porosity and the near-wall radial porosity profile of the full bed [18].

Aside from synthetically-generated beds, imaging methods offer a direct coupling between experimental setups and CFD models [19, 20]. Mantle *et al.* used 3D Magnetic Resonance Imaging (MRI) and MRI velocimetry to characterise the structure and flow field through a packed bed of alumina particles and compare the results with CFD simulations [21]. They observed that flow through the pores was highly heterogeneous, with 40% of fluid flowing through 10% of the pores [21]. Suzuki *et al.* used Computed Tomography (CT) to map the internal structure of modispersed spherical beds [22]. The scans were then used to produce a theoretical correlation to predict radial porosity profiles, based on an amplitude and a damping factor [22].

All these studies reveal that accurate coupling and representation of the experimental bed structure with CFD models is of utmost importance when it comes to solution accuracy. In our previous work, we used CT to characterise the 3D bed structure of three catalytic beds, consisting of 100-300, 300-500, and 500-700 μm SAPO-34 particles, which were produced by sieving, in terms of bulk and radial porosities [23]. By comparing their bulk and radial porosities with those produced by monodispersed spherical beds, significant differences were observed. This is due to the catalytic beds consisting of a wide range of particle sizes, shapes, and orientations, as sieving offered limited control over the particle forms [23]. Producing CFD simulations for these CT-scanned geometries will yield unique observations, as this level of polydispersity cannot be easily achieved with DEM-generated beds. Due to their highly complex topological nature, however, the computational demands associated with meshing these geometries could quickly become prohibitive. Keeping these demands at reasonable levels necessitates the use of smaller bed sections. Here, we investigate the accuracy of representing the full catalytic bed using only a small section, as well as the best meshing setup to achieve mesh independency while reducing the computational demands.

2. Methodology

Work in this paper focuses primarily on the 300-500 and 500-700 μm cases of our previous work [23], which were produced by five passes through the respective sieve fractions. The 100-300 μm case was omitted, as due to the small size of the interparticle pores and the large particle population (≈60k particles), the produced computational mesh was of bad quality, resulting in computational instabilities.

2.1. Representative bed section

As highlighted by both Bai *et al.* [12] and Boccardo *et al.* [18], selecting a suitable section of the entire catalytic bed can be a reasonable approach to reduce the computational demands of particle-resolved models. However, for this section to be an accurate representation, both its bulk and its radial porosity should match those of the full bed as close as possible. To identify this, three sample sections were chosen, corresponding to 5%, 10%, and 50% of the full 300-500 and 500-700 μm beds. These sections span upwards and downwards from the centre of the full bed, as can be seen in Figure 1. Particle colours represent their equivalent diameter metric, as defined in our full bed analysis [23], with blue: 100-300 μm, red: 300-500 μm, green: 500-700 μm, and yellow: >700 μm. Similarly to the full bed, the sections of both geometries consist of a range of particle sizes and shapes.

2.2. Porosity estimation

The method used to estimate the bulk and radial porosities of the full bed was described in detail in our previous work and is repeated here. The binary CT images were fragmentised into concentric rings with a thickness of 0.05 mm, thus creating a radial region along the full bed length. In this area, the "Analyze Particles" function from Fiji ImageJ [24, 25] software was used to quantify the area covered by the particles and compare it to the total area of the concentric

rings. By integrating this area over the entire bed section, the total area covered by the particles, and thus the packing density, can be quantified.

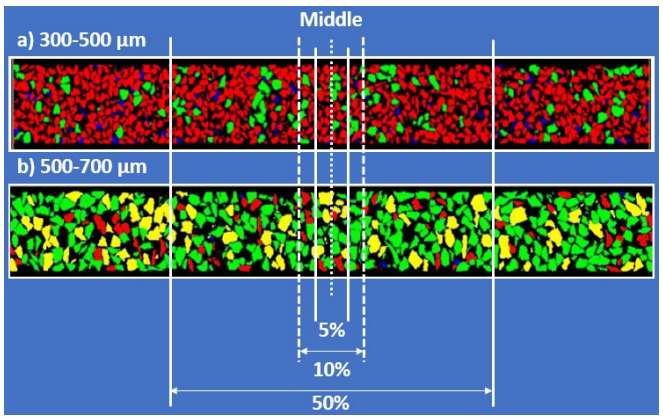

Figure 1: The 5%, 10%, and 50% sections of the a) 300-500 and b) 500-700 µm beds. The CT images refer to the full beds and were produced in our previous work [23].

Table 1: Computational resources of the 10% section of the 300-500 µm bed. Simulations were performed with 2 Intel Xeon 6130 2.1 GHz CPUs with 158 Gb of allocated RAM.

	Coarse	Medium	Refined
Mesh elements	11.0M	18.8M	22.3M
File size [Gb]	1.04	1.8	2.1
Computational time per 100 iterations [sec]	108	361	371
Ram utilisation [Gb]	35.3	68.9	68.7

2.3. Geometry meshing

For this work, meshing was focused solely on the 10% section of the 300-500 µm bed, aiming to identify the mesh size where mesh independency is achieved. Only the interparticle pore space is meshed, while the catalytic particles are neglected, i.e., treated as void, unmeshed regions. The generated CT images contained a significant population of dust particles, i.e., particles smaller than 100 µm. These particles, while numerous, occupy a negligible volume of the full bed [23]. As the focus of our previous study was the accurate characterisation of the bed structure, these particles were maintained. However, meshing the regions surrounding these particles would quickly lead to exhaustive computational meshes, as high local refinement would be necessary to avoid heavily skewed computational cells. Meshing quality and independency are both key for accurate CFD results [18, 26]. Consequently, to preserve the mesh quality and reduce its overall size, dust-like particles were completely removed with the Fiji ImageJ software through a three-step process which involved the Erode, Dilate, and Close functions [25]. In addition, empty fluid regions were added prior and after the catalytic bed, with a length of 0.6 and 1.8 mm respectively, to allow a stable flow during the CFD simulations. Following image processing, meshing was then performed with the Simpleware ScanIP software from Synopsys Inc. Further processing was done in Simpleware, using "Island Removal", to remove unconnected particles smaller than 60 µm. Meshing was performed with the +FE Free algorithm. This algorithm uses adaptive tetrahedral elements to preserve the small features and the complex topological structure within the porous region [27]. To identify mesh independency, three refinement levels are considered by controlling the coarseness of the +FE Free algorithm, with the characteristics of the produced meshes being presented in Table 1.

2.3. Solution setup

The hydrodynamics of the 10% 300-500 µm bed section were resolved using the 3D double precision ANSYS Fluent v22.2 solver. Fluent solves the mass and momentum conservation equations of the fluid in their steady-state, laminar form [28]. Air flow at atmospheric pressure and ambient temperature was considered, while the direction of the gravitational acceleration follows the flow path, i.e., from inlet to outlet. The SIMPLE algorithm was used for pressure-velocity coupling, with a Second Order upwind scheme. Under-relaxation factors of 0.5 were used for pressure and momentum, while residual targets were set to 1e-4. Solution proceeded until convergence or until 4000 iterations had passed. All cases were simulated on the IRIDIS 5 high performance computing facility, utilising 2 Intel Xeon 6130 2.1 GHz CPU, with 158 Gb of allocated

RAM. The computational resources, estimated as computational time necessary for 100 iterations to be resolved, and as RAM utilisation, are also presented in Table 1.

3. Results

3.1. Porosity profiles

The radial and bulk porosities of the different bed sections of the 300-500 and 500-700 μm cases are presented in Figure 2a and b, respectively. As a reference, respective data for the full bed cases are also presented, as per [23]. For both cases, the smaller the bed section, the larger the deviation in both the radial and the bulk porosity. For the 300-500 μm case, the 50% section accurately reproduces the first and second radial porosity oscillations near the container wall; however, deeper into the bed, its oscillations present larger amplitudes compared to the full bed's profile. Furthermore, its bulk porosity is very close to that of the full bed, with a deviation of 0.5%. On the contrary, the 5% section presents very large oscillations along the entire radial length. Especially in the near-centre region, there is a significant resurgence of oscillations, reaching a porosity of almost 0.77 in the bed centre. This confirms the observations from our previous work [23], that, when the bed is broken down into smaller sections, its structure is highly heterogeneous, while when a global radial porosity is derived, its profile appears smooth. Due to this largely empty region in the bed centre, channelling flow could take place, similarly to what is observed for the near-wall regions, allowing the flow to move through the pores uninterrupted [8, 29]. For spherical beds, such empty channels in the centreline of the bed are only observed for small container-to-particle diameter ratios, i.e., $N \leq 2.6$ [5]. The 300-500 μm case, however, has a N-ratio around 10, thus such topological structures are not expected. The 5% section confirms that large heterogeneities in particle sizes, shapes, and orientations, can locally generate large gaps, resulting in flow profiles that would be significantly different than those of monodispersed spherical beds. The bulk porosity of the 5% section also deviates significantly from the full bed case. The 10% section has a radial profile in-between the 5% and 50% sections, also showcasing resurgence of oscillations in the near-centre region. However, the overall trend of the full bed case is captured, while its bulk porosity is the closest to the full bed case, with an error of 0.2%.

On the contrary, for the 500-700 μm case, both the 5% and the 10% sections have very similar radial profiles, producing oscillations with considerably larger amplitudes and periods compared to the full bed case. The 50% section produces a radial profile which is very close to that of the full bed along the majority of the radial length but showcases a resurgence in oscillations near the bed centre. The bulk porosity follows an inverse trend with the bed section, with the smallest error, equal to 1.4%, being produced by the 50% section and the biggest error, equal to 3.5%, being produced by the 5% section. These results are indicative of the relationship between bed structure heterogeneity and particle size. As the size of the particles is increased, and with them being deposited at various random orientations, bigger local interparticle pores are created. Consequently, bulk porosity is then increased from 44% (300-500 μm) to 46% (500-700 μm). The increase of empty pores is also evident by examining the black regions of Figure 1b.

Because of the highly heterogeneous nature of these beds, selection of the most suitable sample section is case dependent. For the 300-500 μm case, while the 10% section does not reproduce the radial profiles as accurately as the 50% section, it gives a satisfactory representation of the full bed. As a result, and with the goal of reducing the computational mesh size, it is chosen as a suitable section to study the flow profiles. For the 500-700 μm case, however, the 10% section produces very large oscillations, while the error in the bulk porosity is rather large, equal to 2.9%. As a result, the 50% section would be a more suitable candidate. In this work, meshing and CFD simulations are performed solely for the 300-500 μm case, while comparison of the two bed cases is planned for our future work.

3.1. Mesh independency

Mesh independency is evaluated through the velocity magnitude and pressure profiles. Figure 3a compares the average velocity magnitude of the different meshes at the concentric rings used to estimate the bed's radial porosity of Figure 2, integrated over the entire radial length of the bed. Figure 3b compares the average velocity magnitude of the different meshes integrated over various axial lengths, each with an axial thickness of 0.05% of the total bed section length.

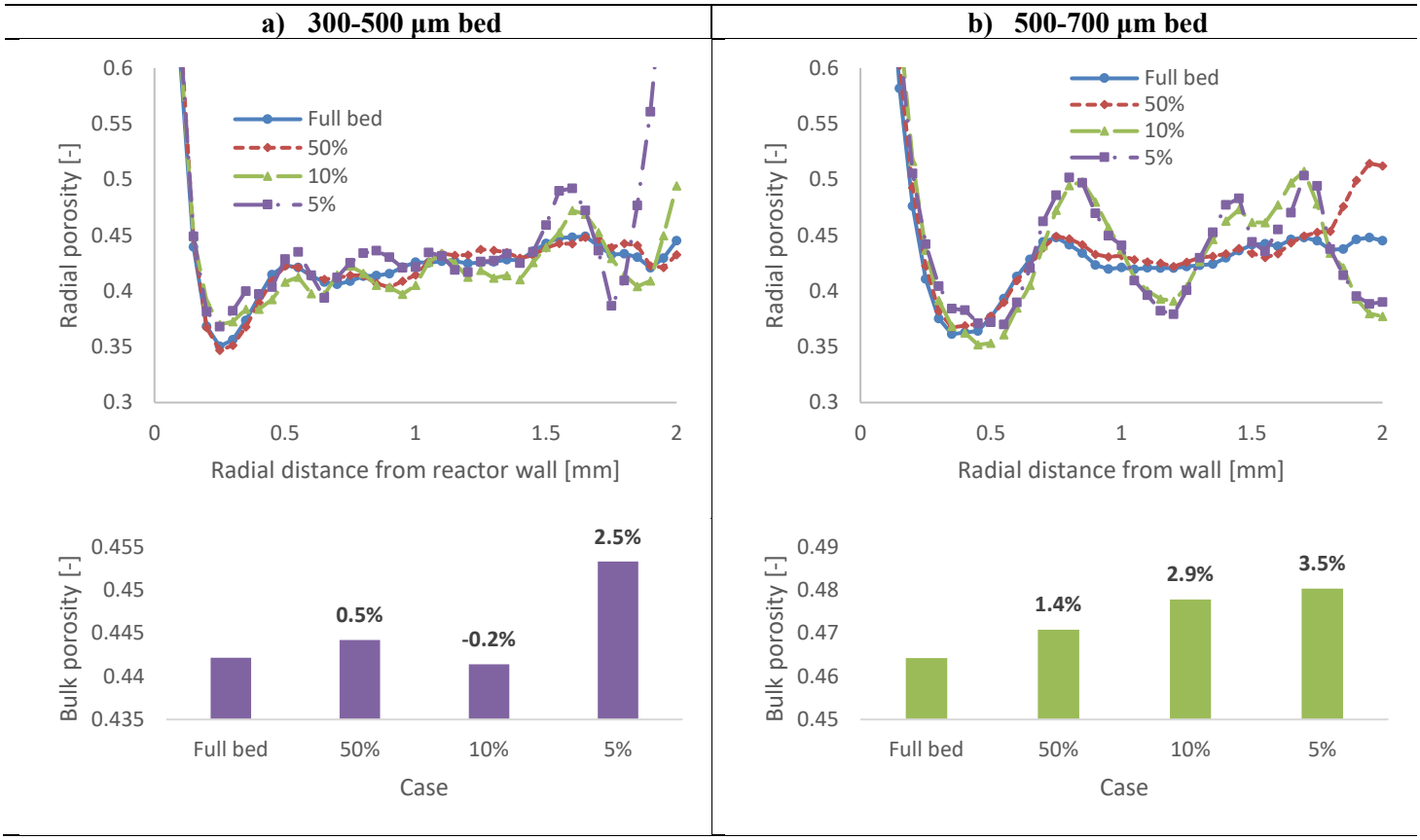

Figure 2: Radial and bulk porosity of a) the 300-500 and b) 500-700 µm cases, as a result of the bed section selected

The differences in the velocity magnitude profiles clearly indicate the solution accuracy achieved as the mesh is further refined. Mesh independency has been achieved at the medium refinement level, as its results are identical to those of the refined mesh for both the radial and the axial velocity profiles. For the coarse mesh, the flow results are very close to those of the other two cases, with the trends being accurately reproduced. Noticeably, however, the local region at a radial distance of around 0.25 mm from the wall (i.e., around half a particle diameter) is not accurately resolved with the coarse mesh. Similarly, along the axial profiles, the sharp velocity peaks and gradients of the medium and refined meshes are not always reproduced by the coarse mesh. With the topological features of the CT geometries being highly complex, containing narrow gaps which are formed in-between neighbouring particles, the coarse mesh cannot accurately discretise them, thus introducing errors in the flow profiles. As a result, the average error between the coarse and the refined mesh cases is around 1.6% and 1.0% for the radial and axial velocity profiles, respectively.

The radial and axial pressure profiles for the same respective regions are presented in Figure 4a and b, respectively. Similarly to the velocity profiles, the pressure profiles between the medium and the refined meshes are identical, further supporting that mesh independency has been reached. While capturing the overall trend, the coarse mesh predicts a lower pressure magnitude, both along the radial and the axial profiles. Specifically, compared to the refined mesh, the coarse mesh produced an average error of 6.9% and 6.2% for the radial and axial pressure profiles, respectively. The discrepancies in the velocity magnitude profiles around the radial distance of 0.25 mm from the wall are also noticed here, expressed as a local pressure decrease, as per Figure 4a.

With the available data, it becomes evident that selection of both a suitable bed section and a suitable mesh refinement level are key for accurate CFD results. A 50% section for both the 300-500 and 500-700 µm cases, combined with a medium refined mesh, would lead to the most accurate results. Unfortunately, computational resources are a considerable limitation

that should be taken into account. If the 50% section of the 300-500 μm bed was instead meshed, and a linear increase of the computational resources of Table 1 was assumed, then mesh size and file size would be increased to 55M/5.2 Gb and 94M/8.9 Gb for the coarse and medium refinement levels, respectively. With such an increase, case setup, computational solution, and result processing would be a challenging task even for cluster-level machines. In fact, a linear increase of the complex mesh with the bed section is a conservative scenario; due to its topological complexity, expecting an exponential increase would be far more realistic. Furthermore, the current geometry only resolves the interparticle pore space and solely considers the mass and momentum conservation equations. The size of the computational mesh would double with the inclusion of the catalytic particles in the 3D geometry, while solution of the energy and species conservation equations, which will provide an overview of the heat transfer and chemical reactions, would significantly increase the computational time and file size. These considerations highlight that simplifications and assumptions are inevitable. Consequently, based on the considered study, computational engineers should balance the level of detail required, the computational resources available, and the maximum acceptable error, to reach a decision on the most suitable CFD setup. With velocity and pressure presenting significant local changes in their magnitudes, understanding the flow field within highly polydispesed beds will produce valuable observations for reactor engineering, aimed at efficiently utilising the catalyst and maximising the product yield.

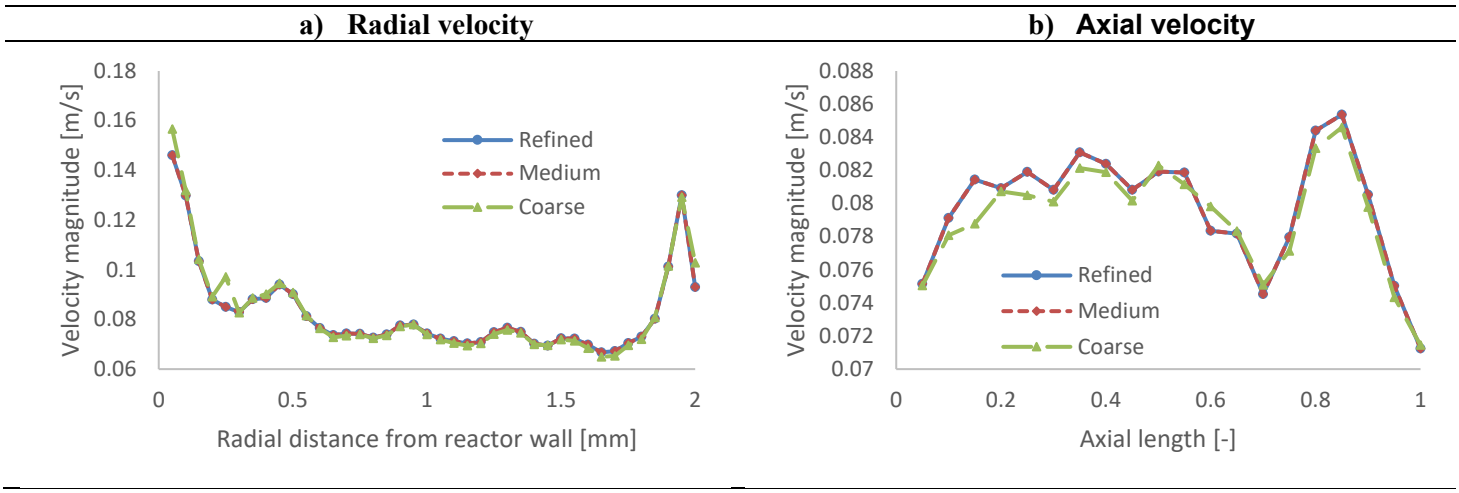

Figure 3: a) Radial and b) axial velocity magnitude profiles of the 10% 300-500 μm bed section with different mesh refinement levels

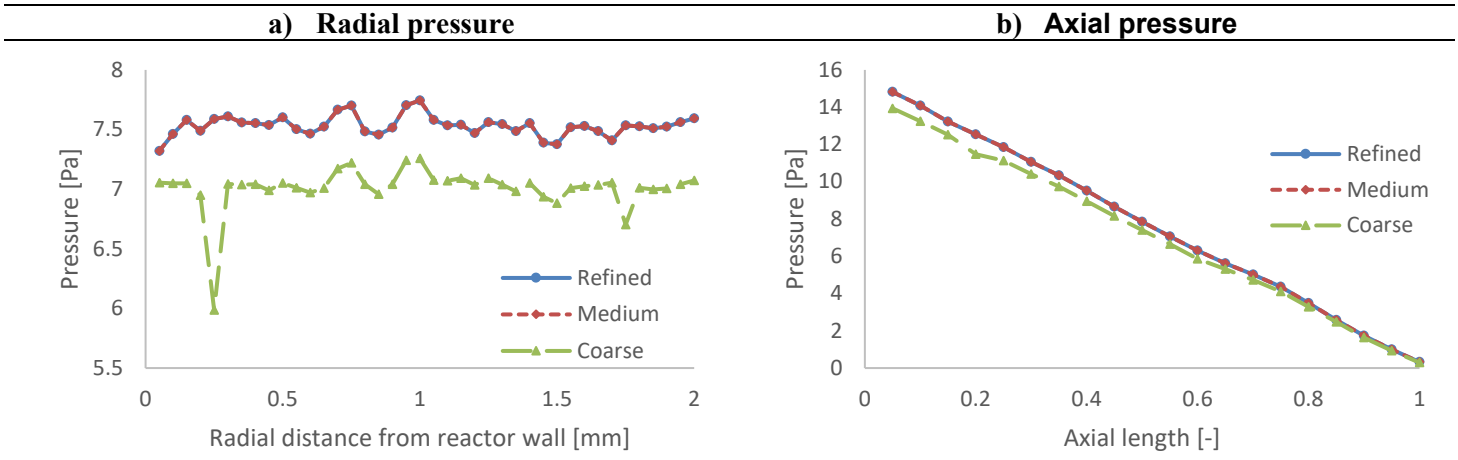

Figure 4: a) Radial and b) axial pressure profiles of the 10% 300-500 μm bed section with different mesh refinement levels

4. Conclusions

Combining imaging methods which map the internal structure of catalytic fixed bed reactors, such as computed tomography (CT), with computational fluid dynamics (CFD) solvers, allows for a unique coupling between experimental setups and simulation models. Unlike synthetically-generated mono- or polydispersed beds, CT-scans are able to directly translate the experimental reactor into a 3D geometry, available for meshing and simulating. In our previous work, fixed bed reactors consisting of 300-500 and 500-700 μm SAPO-34 particles were scanned through CT, allowing the analysis of their internal structure. Due to their polydispersed nature, particles of a wide range of sizes, shapes, and orientations were observed, creating complex topological arrangements.

Meshing and simulating these structures could quickly lead to exhaustive computational demands, thus necessitating the selection of smaller sample sections. For these sections to be suitable, however, they should match the structural morphology of the full bed. To quantify this, three sections were chosen, equal to 5%, 10%, and 50% of the full bed. It was observed that, due to the high irregularity of the bed structure, a suitable sample section is case-dependent. For the 300-500 μm case, a section of 10% is suitable, as it is an acceptable representation of the full bed, in terms of radial and bulk porosities. Due to its highly irregular nature, however, for the 500-700 μm case, a 50% section of the total bed is more suited compared to a 10% section. The selected 10% section of the 300-500 μm case was then meshed, and a mesh independency study was performed by solving the mass and momentum conservation equations. Choosing a coarser mesh introduces an error of around 1.6% and 6.9% in the radial velocity and pressure profiles, respectively, as local topological structures are not accurately resolved, but its computational resources are greatly reduced compared to more refined meshes. These results highlighted the necessity to balance computational demands with solution accuracy.

Acknowledgements

The authors would like to thank the Industrial Decarbonisation Research and Innovation Centre (IDRIC), grant number (EP/V027050/1), for their funding. In addition, the authors would like to acknowledge the use of the IRIDIS 5 High Performance Computing Facility, and associated support services at the University of Southampton, in the completion of this work.

References

[1] A. G. Dixon and B. Partopour, "Computational Fluid Dynamics for Fixed Bed Reactor Design," Annual Review of Chemical and Biomolecular Engineering, vol. 11, no. 1, pp. 109-130, 2020

[2] B. Partopour and A. G. Dixon, "110th Anniversary: Commentary: CFD as a Modeling Tool for Fixed Bed Reactors," Industrial & Engineering Chemistry Research, vol. 58, no. 14, pp. 5733-5736, 2019/04/10 2019

[3] S. Kyrimis, M. E. Potter, R. Raja, and L.-M. Armstrong, "Understanding catalytic CO2 and CO conversion into methanol using computational fluid dynamics," Faraday Discussions, 10.1039/D0FD00136H vol. 230, no. 0, pp. 100-123, 2021

[4] A. G. Dixon, M. Nijemeisland, and E. H. Stitt, "Packed Tubular Reactor Modeling and Catalyst Design using Computational Fluid Dynamics," Computational Fluid Dynamics, vol. 31, pp. 307-389, 2006

[5] J. Theuerkauf, P. Witt, and D. Schwesig, "Analysis of particle porosity distribution in fixed beds using the discrete element method," Powder Technology, vol. 165, no. 2, pp. 92-99, 2006/07/13/ 2006

[6] A. G. Dixon, "Local transport and reaction rates in a fixed bed reactor tube: Exothermic partial oxidation of ethylene," Chemical Engineering Science, vol. 231, p. 116305, 2021/02/15/ 2021

[7] B. Partopour and A. G. Dixon, "Integrated multiscale modeling of fixed bed reactors: Studying the reactor under dynamic reaction conditions," Chemical Engineering Journal, vol. 377, p. 119738, 2019/12/01/ 2019

[8] T. Atmakidis and E. Y. Kenig, "CFD-based analysis of the wall effect on the pressure drop in packed beds with moderate tube/particle diameter ratios in the laminar flow regime," vol. 155, no. 1-2, pp. 404-410, 2009

[9] S. Das, N. G. Deen, and J. A. M. Kuipers, "A DNS study of flow and heat transfer through slender fixed-bed reactors randomly packed with spherical particles," Chemical Engineering Science, vol. 160, pp. 1-19, 2017/03/16/ 2017

[10] J. Tobiś, "Modeling of the Pressure Drop in the Packing of Complex Geometry," Industrial & Engineering Chemistry Research, vol. 41, no. 10, pp. 2552-2559, 2002/05/01 2002
[11] J. Tobiś, "Influence of bed geometry on its frictional resistance under turbulent flow conditions," vol. 55, no. 22, pp. 5359-5366, 2000
[12] H. Bai, J. Theuerkauf, P. A. Gillis, and P. M. Witt, "A Coupled DEM and CFD Simulation of Flow Field and Pressure Drop in Fixed Bed Reactor with Randomly Packed Catalyst Particles," Industrial & Engineering Chemistry Research, vol. 48, no. 8, pp. 4060-4074, 2009/04/15 2009
[13] N. Jurtz, G. D. Wehinger, U. Srivastava, T. Henkel, and M. Kraume, "Validation of pressure drop prediction and bed generation of fixed-beds with complex particle shapes using discrete element method and computational fluid dynamics," AIChE Journal, https://doi.org/10.1002/aic.16967 vol. 66, no. 6, p. e16967, 2020/06/01 2020
[14] G. D. Wehinger, C. Fütterer, and M. Kraume, "Contact Modifications for CFD Simulations of Fixed-Bed Reactors: Cylindrical Particles," Industrial & Engineering Chemistry Research, vol. 56, no. 1, pp. 87-99, 2017/01/11 2017
[15] B. Partopour and A. G. Dixon, "An integrated workflow for resolved-particle packed bed models with complex particle shapes," Powder Technology, vol. 322, pp. 258-272, 2017/12/01/ 2017
[16] A. Pavlišič, R. Ceglar, A. Pohar, and B. Likozar, "Comparison of computational fluid dynamics (CFD) and pressure drop correlations in laminar flow regime for packed bed reactors and columns," Powder Technology, vol. 328, pp. 130-139, 2018/04/01/ 2018
[17] M. Zhang, H. Dong, and Z. Geng, "Computational study of particle packing process and fluid flow inside Polydisperse cylindrical particles fixed beds," Powder Technology, vol. 354, pp. 19-29, 2019/09/01/ 2019
[18] G. Boccardo, F. Augier, Y. Haroun, D. Ferré, and D. L. Marchisio, "Validation of a novel open-source work-flow for the simulation of packed-bed reactors," Chemical Engineering Journal, vol. 279, pp. 809-820, 2015/11/01/ 2015
[19] G. Boccardo, D. L. Marchisio, and R. Sethi, "Microscale simulation of particle deposition in porous media," Journal of Colloid and Interface Science, vol. 417, pp. 227-237, 2014/03/01/ 2014
[20] M. J. Baker, P. G. Young, and G. R. Tabor, "Image based meshing of packed beds of cylinders at low aspect ratios using 3d MRI coupled with computational fluid dynamics," Computers & Chemical Engineering, vol. 35, no. 10, pp. 1969-1977, 2011/10/13/ 2011
[21] M. D. Mantle, A. J. Sederman, and L. F. Gladden, "Single- and two-phase flow in fixed-bed reactors: MRI flow visualisation and lattice-Boltzmann simulations," Chemical Engineering Science, vol. 56, no. 2, pp. 523-529, 2001/01/01/ 2001
[22] M. Suzuki, T. Shinmura, K. Iimura, and M. Hirota, "Study of the Wall Effect on Particle Packing Structure Using X-ray Micro Computed Tomography," Advanced Powder Technology, vol. 19, no. 2, pp. 183-195, 2008/01/01/ 2008
[23] S. Kyrimis, K. E. Rankin, M. E. Potter, R. Raja, and L.-M. Armstrong, "Towards realistic characterisation of chemical reactors: An in-depth analysis of catalytic particle beds produced by sieving," Advanced Powder Technology, vol. 34, no. 2, p. 103932, 2023/02/01 2023
[24] C. A. Schneider, W. S. Rasband, and K. W. Eliceiri, "NIH Image to ImageJ: 25 years of image analysis," Nature Methods, vol. 9, no. 7, pp. 671-675, 2012/07/01 2012
[25] W. R. Tiago Ferreira, "ImageJ User Guide," ImageJ User Guide IJ 1.46r, October 2012 2012.
[26] J. Blazek, "Chapter 11 - Principles of Grid Generation," in Computational Fluid Dynamics: Principles and Applications (Second Edition), J. Blazek Ed. Oxford: Elsevier Science, 2005, pp. 373-413.
[27] X. Fan, X. Ou, F. Xing, G.A. Turley, P. Denissenko, M.A. Williams, N. Batail, C. Pham, A. A. Lapkin, "Microtomography-based numerical simulations of heat transfer and fluid flow through β-SiC open-cell foams for catalysis," Catalysis Today, vol. 278, pp. 350-360, 2016/12/01/ 2016
[28] ANSYS Inc., "ANSYS Fluent User's Guide," Fluent User's Guide, vol. Release 15.0, November 2013 2013.
[29] R. E. Hayes, A. Afacan, and B. Boulanger, "An equation of motion for an incompressible Newtonian fluid in a packed bed," vol. 18, no. 2, pp. 185-198, 1995